materials

Article

Kinetic and Thermodynamic Study of Methylene Blue Adsorption on TiO_2 and ZnO Thin Films

William Vallejo *, Carlos Enrique Diaz-Uribe and Freider Duran

Grupo de Fotoquímica y Fotobiología, Universidad del Atlántico, Puerto Colombia 81007, Colombia; carlosdiaz@mail.uniatlantico.edu.co (C.E.D.-U.); fgduran@mail.uniatlantico.edu.co.edu.co (F.D.)
* Correspondence: williamvallejo@mail.uniatlantico.edu.co; Tel.: +57-5359-9484

Abstract: In this work, we fabricated and characterized ZnO and TiO_2 thin films, determining their structural, optical, and morphological properties. Furthermore, we studied the thermodynamics and kinetics of methylene blue (MB) adsorption onto both semiconductors. Characterization techniques were used to verify thin film deposition. The semiconductor oxides reached different removal values, 6.5 mg/g (ZnO) and 10.5 mg/g (TiO_2), after 50 min of contact. The pseudo-second-order model was suitable for fitting the adsorption data. ZnO had a greater rate constant (45.4×10^{-3}) than that of TiO_2 (16.8×10^{-3}). The removal of MB by adsorption onto both semiconductors was an endothermic and spontaneous process. Finally, the stability of the thin films showed that both semiconductors maintained their adsorption capacity after five consecutive removal tests.

Keywords: environmental remediation; thermodynamics; adsorption; thin films; TiO_2; ZnO

Citation: Vallejo, W.; Diaz-Uribe, C.E.; Duran, F. Kinetic and Thermodynamic Study of Methylene Blue Adsorption on TiO_2 and ZnO Thin Films. *Materials* **2023**, *16*, 4434. https://doi.org/10.3390/ma16124434

Academic Editors: Maria Luisa Testa and Marco Russo

Received: 11 May 2023
Revised: 9 June 2023
Accepted: 13 June 2023
Published: 16 June 2023

1. Introduction

The world's population growth and the energy and water requirements by industries (e.g., petrochemical [1], pharmaceutical [2], textile [3], agrochemical [4], fuels [5], plastics [6]) have caused a severe threat to the environment. Water pollution makes water unsafe for fauna and humans, affecting different environmental systems [7]. One of the challenges for this century is to ensure that the population has access to safe water; the Organization for Economic Co-operation and Development (OECD) recommends that governments encourage the joint management of water quantity and quality [8]. Various techniques for water remediation have been implemented in the last decades (e.g., physical, chemical, and biological treatment technologies) [9]. Among these methods, the adsorption method (a physical method) has received attention due to its low cost and its effectiveness in removing contaminants from water [10]. During the adsorption process, the pollutant is retained on the substrate surface. Adsorption can be described as a chemical (covalent bond) or physical (weak electrostatic interactions) interaction between an adsorbate and adsorbent surface [11]. Different materials have been used to apply the adsorption process (e.g., zeolites, [12], alumina [13], clay [14], active carbon [15], biomass [16], semiconductors [17], MOF [18]). In the literature, there are various reviews on dye removal by adsorption using different materials [19–21]. Metal oxides have two synergic properties: (i) they can act as an adsorbent and (ii) as antimicrobial agents [22]. Furthermore, because semiconductors have variable oxidation states, large surface areas (e.g., as nanomaterials), and great versatility, they can be used for environmental control and contaminant removal [23]. Khoshhesab et al. reported that nanoparticles of ZnO had 92.3% of adsorption capacity in the removal of Congo red from a solution (75 ppm) after 120 min of contact [24]. Syarif et al. reported that nanoparticles of CuO had 61.0% of adsorption capacity in the removal of methylene blue from a solution (5 ppm) after 10 min of contact with CuO nanoparticles [25]. Noreen et al. utilized Fe_3O_4 nanoparticles to remove a reactive blue dye from a solution, and reported 35 mg/g of adsorption capacity after 10 min of contact [26]. Abdullah et al. prepared MnO_2

nanoparticles to remove methylene blue from an aqueous solution, and reported 22.2 mg/g of adsorption capacity after 60 min of contact [27]. ZnO and TiO_2 are alternative adsorbents, as they are innocuous to the environment, they are chemically and physically stable, and have adequate surface properties (e.g., roughness, porosity, and surface area) [28,29].

Currently, in heterogeneous photocatalysis, as a previous step to the photocatalytic degradation process, the sorption/desorption equilibrium is required. However, the adsorption process studied is not commonly reported in photocatalytic studies [30]. Although there is a high potential of ZnO and TiO_2 as adsorbents, there are few reports on the thermodynamic study of dye adsorption onto the surface of these semiconductors. In this contribution, we synthesized and characterized ZnO and TiO_2 thin films and studied the kinetics and thermodynamics involved in the removal of MB by adsorption onto both thin films.

2. Materials and Methods

2.1. Synthesis and Characterization of Thin Film Deposition

We used ammonium hydroxide and zinc acetate in the synthesis of ZnO powders, according to the procedure described in a previous report [31]. We used Degussa powder (P25) (Sigma-Aldrich, 99.5%, St. Louis, MO, USA) as a source of TiO_2 in the fabrication of TiO_2 thin films, according to the procedure described in a previous report [32]. We immobilized all catalysts on solid substrate to solve problems regarding catalyst removal after finishing the photocatalytic procedure [33]. We utilized the Doctor Blade technique for thin film deposition: First, we prepared a mixture of ZnO or TiO_2 powders, polyethylene glycol (PEG 5000) (Sigma-Aldrich, 99%, St. Louis, MO, USA), isopropyl alcohol (Sigma-Aldrich, 99%, St. Louis, MO, USA), and water. After suspension stabilization, the slurry was loaded into a soda lime substrate by the Doctor Blade method. Finally, the thin films were sintered at 500 °C for 1 h [31,34]. The thin films were characterized by diffuse reflectance spectroscopy measurements, providing information about the optical band gap energy of the semiconductors; by Raman spectroscopy assays, which allowed verifying the presence of ZnO and TiO_2 in the coatings; by X-ray diffraction measurements, which provided information about the crystalline structure of the thin films; and by scanning electron microscopy (SEM) assays, which allowed verifying their morphological properties.

2.2. Adsorption Kinetic and Thermodynamic Study

The semiconductors' films were immersed in a solution of methylene blue—MB (10 mL; 10 mg/L) (Sigma-Aldrich, ≥95%, St. Louis, MO, USA) contained in a glass batch reactor provided with an air bubbling system (0.5 L/min). The reactor was stored in the dark to study the MB adsorption process on the films. An aliquot was extracted at time zero and every 5 min thereafter for 50 min to determine the adsorption–desorption equilibrium time. We determined MB concentration by spectrophotometry at 665 nm using the Lambert–Beer law with a calibration curve (R^2 = 0.997). We determined the adsorption capacity of MB on the semiconductors according to [35]:

$$q_t = \frac{((C_0 - C_t) \cdot V)}{m} \tag{1}$$

where q_t is the amount (mg) of MB adsorbed per gram of semiconductor (mg/g) at each time; C_0 is the initial MB concentration (mg/L); and m (g) is the amount of semiconductor. We applied the pseudo-first-order (PFO) and pseudo-second-order (PSO) models to fit experimental data according to these equations [35]:

$$ln(q_t - q_e) = ln(q_e) - k_1 t \tag{2}$$

$$\frac{t}{q_t} = \frac{1}{k_2 {q_e}^2} + \frac{t}{q_e} \tag{3}$$

where q_t is the amount of MB adsorbed per unit mass of the adsorbent (mg·g^{-1}) at each time; q_e is the maximum sorption capacity (mg ·g^{-1}); and k_1 (min^{-1}) and k_2 (g·mg^{-1}·min^{-1})

are the rate constants of the pseudo-first- and pseudo-second-order models, respectively. The fitting correlation coefficient (R^2) was used to determine the best-fitting kinetic models. Finally, we calculated standard enthalpy ($\Delta H°$), standard entropy ($\Delta S°$), and standard Gibbs free energy ($\Delta G°$) for the adsorption process applying the Arrhenius equation [36]:

$$K = \frac{q_e}{C_e} \tag{4}$$

$$\Delta G^{\circ} = -RTlnK \tag{5}$$

$$lnK = \frac{\Delta S^{\circ}}{R} - \frac{\Delta H^{\circ}}{RT} \tag{6}$$

3. Results

3.1. Raman Characterization

The Raman spectroscopy results are shown in Figure 1. Six Raman-active vibrational modes were observed for TiO_2 in Raman spectroscopy (e.g., A_{1g} + $2B_{1g}$ + $3E_g$) [37]. Three Raman-active vibrational modes were observed for ZnO in Raman spectroscopy (e.g., A_1 + E_1 + E_2) [38]. Both catalysts shows the typical signals reported for such materials [39,40]. For the case of ZnO, the signals located at 274.5 cm^{-1} can be associated with oxygen vacancies into the semiconductor lattice [41,42].

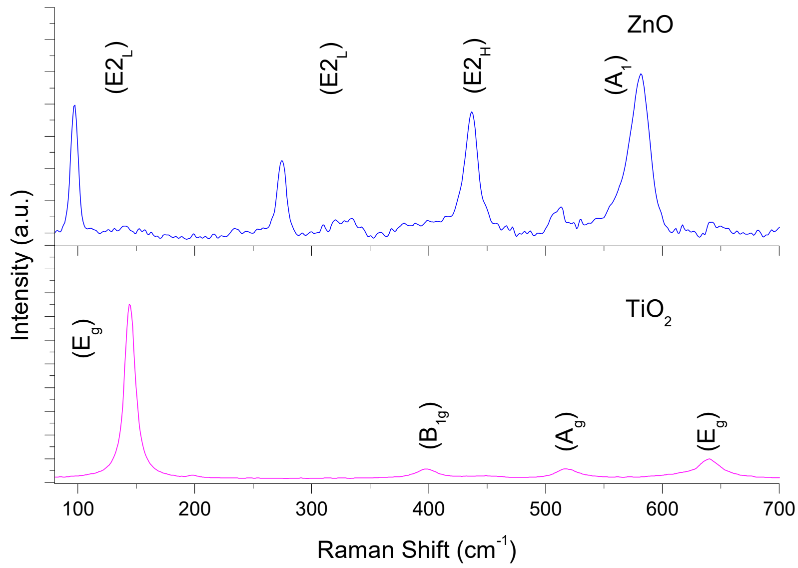

Figure 1. Raman spectrum of ZnO and TiO_2 thin films.

3.2. Structural Characterization

Figure 2 shows the (experimental and simulated) structural results for both TiO_2 and ZnO thin films. ZnO was polycrystalline, whose sample shows a plane of preferential growth located at 2θ = 36.27. This signal is assigned to plane (101), where ZnO thin films show six other preferential growth planes, with all these reflections corresponding to the hexagonal wurtzite phase (JCPDS No. 36−1451) [43]. For the XRD-TiO_2 pattern, the TiO_2 was polycrystalline and was formed by two different crystalline structures: rutile (JCPDS #021-1276) and anatase (JCPDS #071-1166). During thin film deposition, we utilized a TiO_2 source (Degussa-P25), this material being a mixture of those two crystalline phases [44].

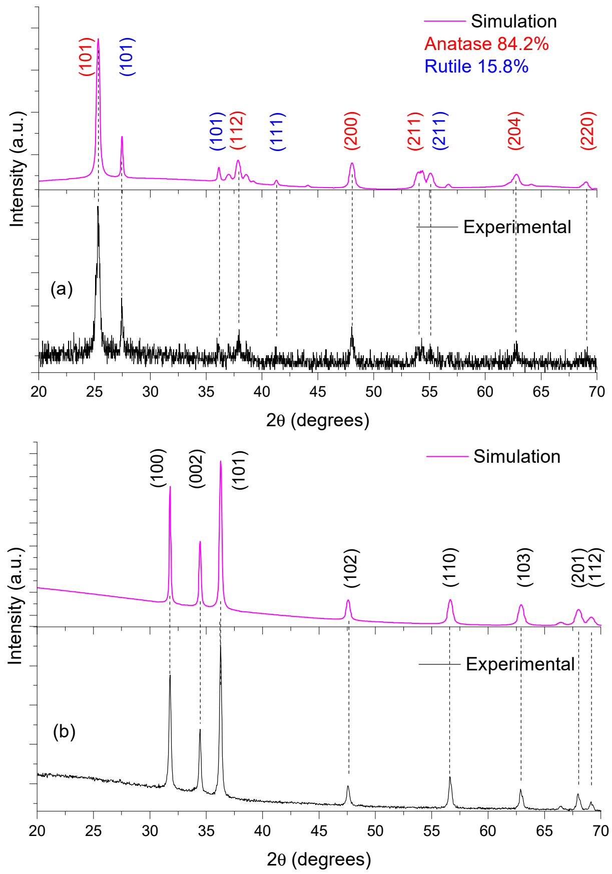

Figure 2. X-ray diffraction data and results of simulation for: (**a**) TiO_2 and (**b**) ZnO.

We utilized a PowderCell package to simulate the experimental XRD data. In the simulation, we employed the rutile and anatase forms of TiO_2, and hexagonal wurtzite (ZnO) crystalline structures. We applied the Rietveld method (Bragg–Brentano geometry with the March–Dollase as model to preferred orientation; with the plane the plane (101) as plane's orientation. The X-ray source was Cu K_α radiation (λ = 0.1544426 nm); the pseudo-Voigt 1 function iterations 300; and the φ factor was 1.9. This methodology was suitable to identify the crystalline phases in each thin film. Table 1 lists the crystalline parameters obtained from the simulations. We employed the Debye–Scherrer equation to determine grain size of the semiconductors [45]. The domain grain size of ZnO was 34.4 nm, and 24.1 nm and 38.8 nm for anatase and rutile structures, respectively. These results correspond to those of previous reports by other authors [44,46].

Table 1. Structural properties of the sensitized semiconductor oxides.

Thin Film	Crystalline Plane	Grain Size (nm) [1]	(a) [2]	(c) [2]
ZnO	(101)	34.4	3.2492	5.2044
TiO_2—Anatase (84.2%)	(101)	18.5	3.7859	9.5044
TiO_2—Rutile (15.8%)	(110)	65.3	4.5922	2.9568

[1] Obtained from applied Debye–Scherrer equation to data of Figure 2. [2] Obtained from simulation PowderCell package.

3.3. Morphological Characterization

Morphological properties are determined by the experimental conditions and deposition method [47]. We synthesized ZnO using the sol–gel method, and we utilized Degussa P25 as the TiO_2 source. Figure 3 shows the morphological results for TiO_2 and ZnO. These results show that the thin films' surfaces are heterogeneous and porous, that TiO_2 and ZnO are composed of microaggregates of different sizes, and that the agglomerated particles have two different spherical sized (50–80 nm to TiO_2 and ~220nm to ZnO). Figure 3a shows typical morphological properties for Degussa P25 TiO_2 [48]. The quasi-spherical ZnO nanoparticles are a commonly reported result when the sol–gel method is employed as a synthesis method [49]. Various authors have reported that the surface properties of the semiconductors are affected by synthesis method employed for their fabrication [23].

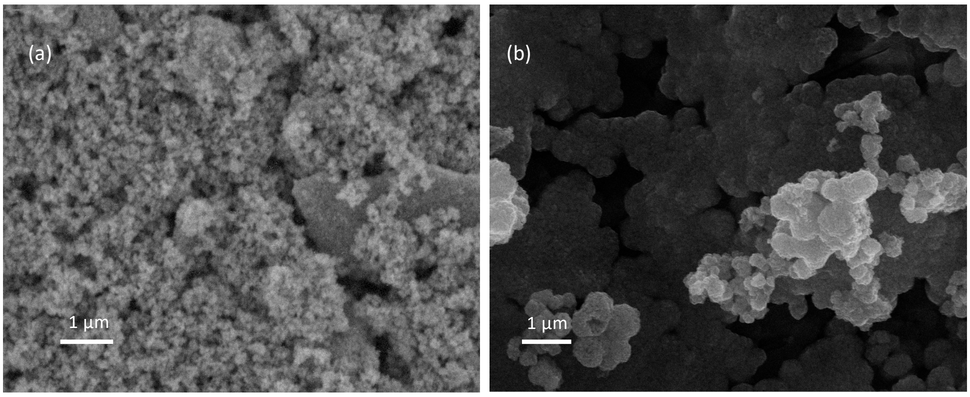

Figure 3. SEM images: (**a**) TiO_2 thin films (×10,000); (**b**) ZnO thin films (×10,000).

3.4. Spectroscopic Characterization

Figure 4 shows optical results for the ZnO and TiO_2 semiconductors. Both of them show a high reflectance of approximately (or greater than) 60% after 360 nm. ZnO and TiO_2 are not active under visible irradiation due to their high band gap (E_g). We determined the E_g value using the Kubelka–Munk remission function [50]. Figure 4b shows the E_g estimation for each thin film. The estimated bad gaps for the thin films are shown in Figure 4b [51]. These results correspond to those of previous reports for ZnO and TiO_2 Degussa P25 [52,53]. The spectroscopic and structural characterization verified the presence of ZnO and TiO_2 in the coatings synthesized.

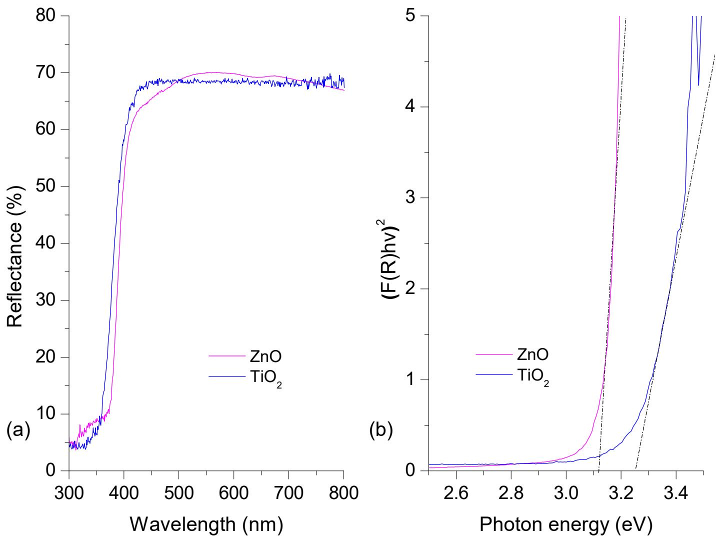

Figure 4. (**a**) TiO_2 and ZnO thin films' diffuse reflectance spectra; (**b**) Kubelka–Munk plots.

3.5. Adsorption Kinetic Study

The adsorption of dye onto a semiconductor surface is a principle that relies on two steps: (i) diffusion of reactants onto the semiconductor surface and (ii) adsorption of reactants onto the semiconductor surface. The first step (the diffusion process) (i) follows the classic laws of diffusion (e.g., Fick's law) [54]. The second step (the adsorption process) (ii) can be a physical or a chemical process. During chemisorption, the dye molecule or ion attaches itself to a specific surface by a chemical bond and, in the physical adsorption, the dye molecules attach onto the adsorbent surface under the influence of van der Waals forces and hydrogen bonding [55]. The adsorption kinetic process can be studied through various theoretical methods (e.g., pseudo-first, pseudo-second, the intraparticle diffusion, Elovich) [35].

Figure 5a,b shows the adsorption kinetics on TiO_2 and ZnO. Figure 5 indicates that the TiO_2 thin films reach 10.5 mg/g and the ZnO thin films reach 6.5 mg/g after 50 min of contact. These differences can be assigned to morphological properties and grain size. Table 2 lists the fitting results of the two models implemented. Table 2 indicates that the PSO model showed was suitable (greatest R value) to describe the adsorption process for both semiconductors. ZnO has a greater k_2 value than that of TiO_2 and a smaller q_e value than that of TiO_2, thus indicating that the ZnO surface saturates faster than the TiO_2 surface, a behavior that can be associated to reduced grain size of TiO_2 thin films. In the PSO model, the electrostatic interaction onto the surface affects the interaction with MB molecules. The MB dye is a cationic dye; the isoelectric point of TiO_2 in water (7.0 [56]) is smaller than the isoelectric point of ZnO (9.5 [57]); and under experimental conditions, the ZnO surface is positively charged, then TiO_2 would have more effective interaction with MB than ZnO thin films would. Furthermore, the grain size of TiO_2 (anatase 84.2%) is smaller than that of ZnO (see Table 1), and the specific surface area of TiO_2 should be greater than that of ZnO, increasing the MB adsorption capacity of TiO_2 in comparison with that of ZnO thin films [58].

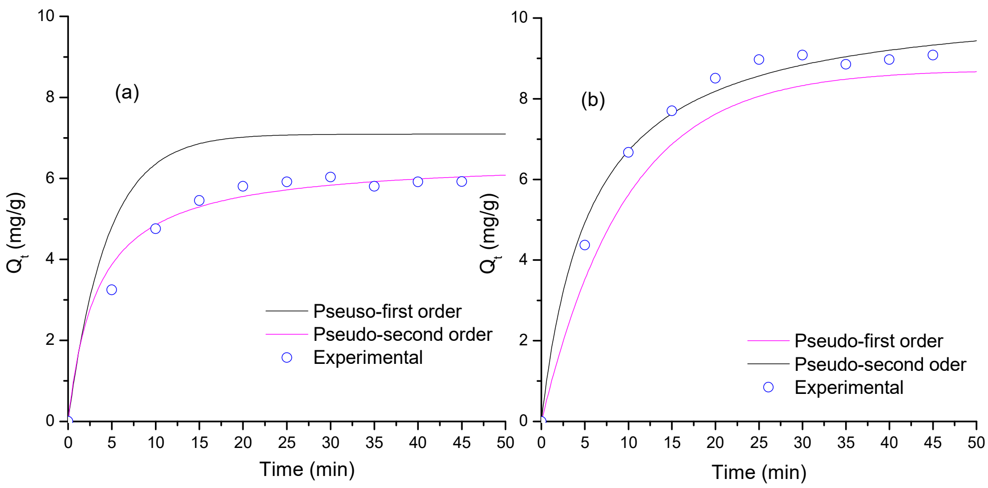

Figure 5. Adsorption kinetics and theoretical fitting of MB adsorption on thin films of the semiconductor oxides (**a**) ZnO and (**b**) TiO_2.

Table 2. Kinetic results for MB adsorption on the semiconductor oxides sensitized.

Thin Film/ Model	1st Order *			2nd Order *		
	qe (mg g−1)	k1 (min−1) × 10−3	R2	qe (mg/g)	k2 (g mg−1min−1) × 10−3	R2
TiO_2	6.89	112	0.885	10.5	16.8	0.993
ZnO	7.09	226	0.877	6.49	45.4	0.995

* Obtained from data in Figure 5.

The adsorption capacities (AC) obtained for ZnO (6.49 mg/g) and TiO_2 (10.5 mg/g) are suitable in comparison with previous reports. Dimauro et al. reported AC values of 7.0 mg/g, 7.4 mg/g, and 7.4 mg/g for MB adsorption onto V_2O_5, V_2O_5/SnO_2, and V_2O_5/TiO_2, respectively [59]. Debnath et al. reported an AC value of 9.6 mg/g for Congo red adsorption onto ZnO nanoparticles [60]. Singh et al. reported an AC value of 7.3 mg/g for MB adsorption onto Fe_3O_4 nanoparticles [61]. Song et. al. reported AC of 8.4 mg/g onto NiO nanoparticles [62]. Konicki et al. reported AC of BY28 and BR46 dyes onto Graphene Oxide was 68.5 and 76.9 mg/g, respectively [63]. Finally, the pseudo-second model has been reported by various authors as a suitable fitting model for dye adsorption on different adsorbent types. Table 3 lists reports fitting kinetic data with pseudo-second model.

3.6. Adsorption Thermodynamic Study

Figure 6 shows the thermodynamic calculation applying the Arrhenius equation to MB adsorption onto the thin films of both semiconductors (Equation (6)). The ΔH° and ΔS° values were calculated from Figure 6. Table 3 lists the thermodynamic results. The removal of MB by using semiconductor oxides was a spontaneous process ($\Delta G < 0$, for both materials). This result is due to the morphological properties of the semiconductors' surface. Furthermore, the adsorption process was endothermic and more stable for TiO_2 than for ZnO. The positive ΔS values of both semiconductor oxides could be associated with a degree of hydration of cationic MB molecules in the solution [64]. The MB remotion was more favored on TiO_2 than on ZnO. Table 3 lists the thermodynamic results reported by other authors. Results show a variation range depending on both adsorbent and dye type. The ΔG° values for all studies listed in Table 3 are negative. It indicates that the dye adsorption onto adsorbents was spontaneous. This spontaneity of the process increases when the temperature increases. Bennabi et. al. reported that this behavior is associated with decreasing thickness of the boundary layer surrounding the adsorbent surface with temperature increasing. This effect improves the mass transfer of the dye to the adsorbent surface [65].

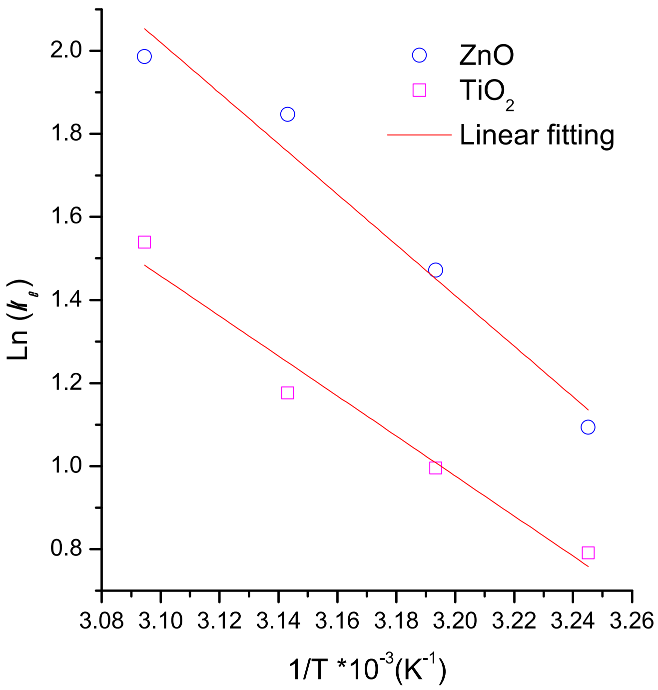

Figure 6. Thermodynamic calculation applying the Arrhenius equation to MB adsorption onto the semiconductor thin films.

Results verified that the adsorption process is an important step and indicated that such a process should be studied during photocatalytic tests.

3.7. Recyclability Study

To verify the potential application of semiconductors in continuous remediation water systems, we determined the recyclability of both semiconductor oxides in the MB adsorption during various cycles. Figure 7 shows the stability results of the studied semiconductors. The adsorption process was repeated five consecutive times. Figure 7 shows that after the fifth cycle, the removal performance reduced by 5% for TiO_2 and 2% for ZnO. Such stable results are associated with the stability of the semiconductor oxides, and with the chemistry of the substrate (soda lime glass) and method of thin film deposition.

These results indicate that the thin films were suitable and reusable for MB adsorption after five cycles.

Table 3. Kinetic results for dye adsorption onto various materials.

Adsorbent/Dye	Temperature	Termodynamic Parameters		
		ΔG (kJ/mol)	ΔH (kJ/mol)	ΔS (J/mol)
* TiO_2 (this work)	308 313 318 323	−2.90 −3.78 −4.65 −5.51	50.6	173
* ZnO (this work)	308 313 318 323	−7.12 −7.89 −8.65 −9.41	40.0	153
Graphene oxide/BY28 [63]	293 313 333	−1.69 −3.58 −5.47	2.74	16.5
NiO/Methyl orange [66]	303 318 333	−2.12 −2.41 −2.79	36.5	126
CuO/Methyl orange [66]	303 318 333	−1.65 −2.52 −3.38	15	58
Cu(I)−PANI/Orange16 [67]	303 308 313 318 323	−8.60 −8.77 −8.94 −9.11 −9.27	1.51	33.4
CdO/Congo Red [63]	298	−11.5	−−	−−
Chitosan/Congo Red [68]	298 308 318 328	−0.55 −2.45 −3.19 −2.41	34.5	118
Biochar/MB [69]	308 313 318 323	−0.95 −1.34 −1.74 −2.14	23.5	79.5
Actived carbon/MB [70]	298 308 318	−1.71 −1.91 −2.91	16.3	60.0
Biomass/MB [71]	298 308 318	−16.6 −19.6 −22.6	72.0	297

* Obtained from data of Figure 6.

These results are relevant to improve continuous flow remediation systems where adsorbents are incorporated in suspension form. Thin films can avoid additional separation steps, reducing the economic implementation of these systems.

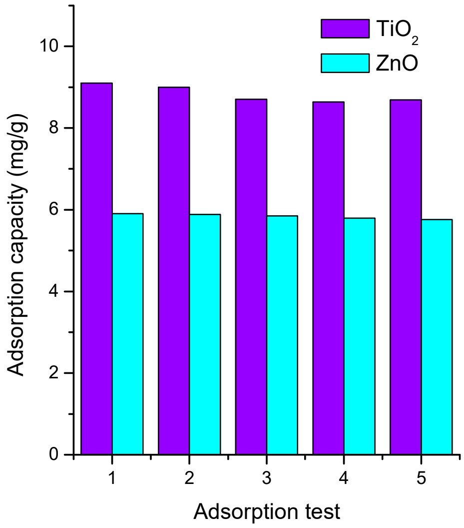

Figure 7. Stability test for MB adsorption onto TiO_2 and ZnO.

4. Conclusions

We fabricated ZnO and TiO_2 thin films. The morphological, optical, and spectroscopic characterizations verified the presence of ZnO and TiO_2 in the coatings. Furthermore, the XRD simulation identified the crystalline structures of both semiconductors: TiO_2 (anatase 84.2%—rutile 15.8%) and ZnO (wurtzite). The pseudo-second-order model was suitable to fit the kinetic results. Furthermore, TiO_2 (q_e 10.5 mg/g) was more effective in MB removal than ZnO (q_e 6.5 mg/g). The MB adsorption onto both semiconductors was a spontaneous and endothermic process: TiO_2 ($\Delta G = -2.9$ kJ/mol; $\Delta H = 50.6$ kJ/mol) and ZnO ($\Delta G = -7.1$ kJ/mol; $\Delta H = 40.0$ kJ/mol). Finally, the recycling test showed that the semiconductors were suitable after five consecutive adsorption tests. All the above results verified the significance of the adsorption process. The present authors consider that adsorption studies should be included during photocatalytic tests.

Author Contributions: Conceptualization, W.V.; methodology, W.V., C.E.D.-U. and F.D.; validation, W.V., C.E.D.-U. and F.D.; formal analysis, W.V., C.E.D.-U. and F.D.; investigation, W.V., C.E.D.-U. and F.D.; resources, W.V., C.E.D.-U. and F.D.; data curation, W.V., C.E.D.-U. and F.D.; writing—original draft preparation, W.V., C.E.D.-U. and F.D., writing—review and editing, W.V., C.E.D.-U. and F.D.; visualization, W.V., C.E.D.-U. and F.D.; supervision, W.V., C.E.D.-U. and F.D.; project administration, W.V., C.E.D.-U. and F.D.; funding acquisition, W.V., C.E.D.-U. and F.D. All authors have read and agreed to the published version of the manuscript.

Funding: This research was funded by Universidad del Atlántico, research project CB398-Cll2022.

Institutional Review Board Statement: Not applicable.

Informed Consent Statement: Not applicable.

Data Availability Statement: All relevant data are available within the article.

Acknowledgments: The authors would like to thank Universidad del Atlántico.

Conflicts of Interest: The authors declare no conflict of interest.

References

1. Tian, X.; Song, Y.; Shen, Z.; Zhou, Y.; Wang, K.; Jin, X.; Han, Z.; Liu, T. A comprehensive review on toxic petrochemical wastewater pretreatment and advanced treatment. *J. Clean. Prod.* **2020**, *245*, 118692. [CrossRef]
2. Ehsan, M.N.; Riza, M.; Pervez, M.N.; Khyum, M.M.O.; Liang, Y.; Naddeo, V. Environmental and health impacts of PFAS: Sources, distribution and sustainable management in North Carolina (USA). *Sci. Total Environ.* **2023**, *878*, 163123. [CrossRef] [PubMed]
3. Ambigadevi, J.; Senthil Kumar, P.; Vo, D.V.N.; Hari Haran, S.; Srinivasa Raghavan, T.N. Recent developments in photocatalytic remediation of textile effluent using semiconductor based nanostructured catalyst: A review. *J. Environ. Chem. Eng.* **2021**, *9*, 104881. [CrossRef]

4. Pandey, S.; Giri, V.P.; Tripathi, A.; Bajpai, R.; Sharma, D.; Bahadur, L.; Mishra, A. Interaction, fate and risks associated with nanomaterials as fertilizers and pesticides. In *Advances in Nano-Fertilizers and Nano-Pesticides in Agriculture*; Woodhead Publishing: Sawston, UK, 2021; pp. 229–248.
5. Ukaogo, P.O.; Ewuzie, U.; Onwuka, C.V. Environmental pollution: Causes, effects, and the remedies. In *Microorganisms for Sustainable Environment and Health*; Elsevier: Amsterdam, The Netherlands, 2020; pp. 419–429.
6. Vaid, M.; Sarma, K.; Gupta, A. Microplastic pollution in aquatic environments with special emphasis on riverine systems: Current understanding and way forward. *J. Environ. Manag.* **2021**, *293*, 112860. [CrossRef]
7. UNESCO. United Nations Educational Scientific and Cultural Organization. In *The United Nations World Water Development Report 2021: Valuing Water*; United Nations: New York, NY, USA, 2021; ISBN 978-92-3-100434-6.
8. OECD. *Groundwater Allocation: Managing Growing Pressures on Quantity and Quality*; OECD Publishing: Paris, France, 2017; ISBN 978-92-6-428155-4.
9. Speight, J.G. Remediation technologies. In *Natural Water Remediation—Chemistry and Technology*; Elsevier: Amsterdam, The Netherlands, 2020; pp. 263–303. [CrossRef]
10. Madhav, S.; Ahamad, A.; Singh, P.; Mishra, P.K. A review of textile industry: Wet processing, environmental impacts, and effluent treatment methods. *Environ. Qual. Manag.* **2018**, *27*, 31–41. [CrossRef]
11. Al-Ghouti, M.A.; Da'ana, D.A. Guidelines for the use and interpretation of adsorption isotherm models: A review. *J. Hazard. Mater.* **2020**, *393*, 122383. [CrossRef] [PubMed]
12. Dryaz, A.R.; Shaban, M.; AlMohamadi, H.; Al-Ola, K.A.A.; Hamd, A.; Soliman, N.K.; Ahmed, S.A. Design, characterization, and adsorption properties of Padina gymnospora/zeolite nanocomposite for Congo red dye removal from wastewater. *Sci. Rep.* **2021**, *11*, 21058. [CrossRef]
13. Banerjee, S.; Dubey, S.; Gautam, R.K.; Chattopadhyaya, M.C.; Sharma, Y.C. Adsorption characteristics of alumina nanoparticles for the removal of hazardous dye, Orange G from aqueous solutions. *Arab. J. Chem.* **2019**, *12*, 5339–5354. [CrossRef]
14. Kausar, A.; Iqbal, M.; Javed, A.; Aftab, K.; Nazli, Z.i.H.; Bhatti, H.N.; Nouren, S. Dyes adsorption using clay and modified clay: A review. *J. Mol. Liq.* **2018**, *256*, 395–407. [CrossRef]
15. Nizam, N.U.M.; Hanafiah, M.M.; Mahmoudi, E.; Halim, A.A.; Mohammad, A.W. The removal of anionic and cationic dyes from an aqueous solution using biomass-based activated carbon. *Sci. Rep.* **2021**, *11*, 8623. [CrossRef]
16. Diaz-Uribe, C.; Angulo, B.; Patiño, K.; Hernández, V.; Vallejo, W.; Gallego-Cartagena, E.; Romero Bohórquez, A.R.; Zarate, X.; Schott, E. Cyanobacterial Biomass as a Potential Biosorbent for the Removal of Recalcitrant Dyes from Water. *Water* **2021**, *13*, 3176. [CrossRef]
17. Sajid, M.M.; Shad, N.A.; Javed, Y.; Khan, S.B.; Zhang, Z.; Amin, N.; Zhai, H. Preparation and characterization of Vanadium pentoxide (V_2O_5) for photocatalytic degradation of monoazo and diazo dyes. *Surf. Interfaces* **2020**, *19*, 100502. [CrossRef]
18. Uddin, M.J.; Ampiaw, R.E.; Lee, W. Adsorptive removal of dyes from wastewater using a metal-organic framework: A review. *Chemosphere* **2021**, *284*, 131314. [CrossRef]
19. Yagub, M.T.; Sen, T.K.; Afroze, S.; Ang, H.M. Dye and its removal from aqueous solution by adsorption: A review. *Adv. Colloid Interface Sci.* **2014**, *209*, 172–184. [CrossRef]
20. Dutta, S.; Gupta, B.; Srivastava, S.K.; Gupta, A.K. Recent advances on the removal of dyes from wastewater using various adsorbents: A critical review. *Mater. Adv.* **2021**, *2*, 4497–4531. [CrossRef]
21. Rana, A.; Qanungo, K. Orange G dye removal from aqueous-solution using various adsorbents: A mini review. *Mater. Today Proc.* **2021**, *81*, 754–757. [CrossRef]
22. Himly, M.; Geppert, M.; Duschl, A. Biological Activity of Metal Oxide Nanoparticles. *Met. Oxide Nanopart.* **2021**, *2*, 735–759.
23. Hosny, N.M.; Gomaa, I.; Elmahgary, M.G. Adsorption of polluted dyes from water by transition metal oxides: A review. *Appl. Surf. Sci. Adv.* **2023**, *15*, 100395. [CrossRef]
24. Monsef Khoshhesab, Z.; Souhani, S. Adsorptive removal of reactive dyes from aqueous solutions using zinc oxide nanoparticles. *J. Chin. Chem. Soc.* **2018**, *65*, 1482–1490. [CrossRef]
25. Syarif, D.; Aliah, H.; Usman, J.; Pratiwi, Y. Synthesis of CuO Nanoparticles for Adsorbent of Methylene Blue. In Proceedings of the 1st International Conference on Islam, Science and Technology, ICONISTECH 2019, Bandung, Indonesia, 11–12 July 2019; European Alliance for Innovation: Bandung, Indonesia, 2021; pp. 1–16.
26. Noreen, S.; Mustafa, G.; Ibrahim, S.M.; Naz, S.; Iqbal, M.; Yaseen, M.; Javed, T.; Nisar, J. Iron oxide (Fe_2O_3) prepared via green route and adsorption efficiency evaluation for an anionic dye: Kinetics, isotherms and thermodynamics studies. *J. Mater. Res. Technol.* **2020**, *9*, 4206–4217. [CrossRef]
27. Abdullah, T.A.; Rasheed, R.T.; Juzsakova, T.; Al-Jammal, N.; Mallah, M.A.; Cuong, L.P.; Salman, A.D.; Domokos, E.; Ali, Z.; Cretescu, I. Preparation and characterization of MnO_2-based nanoparticles at different annealing temperatures and their application in dye removal from water. *Int. J. Environ. Sci. Technol.* **2021**, *18*, 1499–1512. [CrossRef]
28. Heinonen, S.; Nikkanen, J.P.; Huttunen-Saarivirta, E.; Levänen, E. Investigation of long-term chemical stability of structured ZnO films in aqueous solutions of varying conditions. *Thin Solid Film.* **2017**, *638*, 410–419. [CrossRef]
29. Dell'Edera, M.; Lo Porto, C.; De Pasquale, I.; Petronella, F.; Curri, M.L.; Agostiano, A.; Comparelli, R. Photocatalytic TiO2-based coatings for environmental applications. *Catal. Today* **2021**, *380*, 62–83. [CrossRef]

30. Díaz-Uribe, C.; Vallejo, W.; Campos, K.; Solano, W.; Andrade, J.; Muñoz-Acevedo, A.; Schott, E.; Zarate, X. Improvement of the photocatalytic activity of TiO2 using Colombian Caribbean species (*Syzygium cumini*) as natural sensitizers: Experimental and theoretical studies. *Dye. Pigment.* **2018**, *150*, 370–376. [CrossRef]
31. Vallejo, W.; Cantillo, A.; Dias-Uribe, C. Methylene Blue Photodegradation under Visible Irradiation on Ag-Doped ZnO Thin Films. *Int. J. Photoenergy* **2020**, *2020*, 112. [CrossRef]
32. Diaz-Uribe, C.; Vallejo, W.; Camargo, G.; Muñoz-Acevedo, A.; Quiñones, C.; Schott, E.; Zarate, X. Potential use of an anthocyanin-rich extract from berries of Vaccinium meridionale Swartz as sensitizer for TiO_2 thin films—An experimental and theoretical study. *J. Photochem. Photobiol. A Chem.* **2019**, *384*, 112050. [CrossRef]
33. Diaz-Uribe, C.; Vallejo, W.; Ramos, W. Methylene blue photocatalytic mineralization under visible irradiation on TiO_2 thin films doped with chromium. *Appl. Surf. Sci.* **2014**, *319*, 121–127. [CrossRef]
34. Quiñones, C.; Ayala, J.; Vallejo, W. Methylene blue photoelectrodegradation under UV irradiation on Au/Pd-modified TiO_2 films. *Appl. Surf. Sci.* **2010**, *257*, 367–371. [CrossRef]
35. Benjelloun, M.; Miyah, Y.; Akdemir Evrendilek, G.; Zerrouq, F.; Lairini, S. Recent Advances in Adsorption Kinetic Models: Their Application to Dye Types. *Arab. J. Chem.* **2021**, *14*, 103031. [CrossRef]
36. Kayalvizhi, K.; Alhaji, N.M.I.; Saravanakkumar, D.; Mohamed, S.B.; Kaviyarasu, K.; Ayeshamariam, A.; Al-Mohaimeed, A.M.; AbdelGawwad, M.R.; Elshikh, M.S. Adsorption of copper and nickel by using sawdust chitosan nanocomposite beads—A kinetic and thermodynamic study. *Environ. Res.* **2022**, *203*, 111814. [CrossRef] [PubMed]
37. Surmacki, J.; Wroński, P.; Szadkowska-Nicze, M.; Abramczyk, H. Raman spectroscopy of visible-light photocatalyst—Nitrogen-doped titanium dioxide generated by irradiation with electron beam. *Chem. Phys. Lett.* **2013**, *566*, 54–59. [CrossRef]
38. Aljaafari, A. Size Dependent Photocatalytic Activity of ZnO Nanosheets for Degradation of Methyl Red. *Front. Mater.* **2020**, *7*, 362. [CrossRef]
39. Nowak, E.; Szybowicz, M.; Stachowiak, A.; Koczorowski, W.; Schulz, D.; Paprocki, K.; Fabisiak, K.; Los, S. A comprehensive study of structural and optical properties of ZnO bulk crystals and polycrystalline films grown by sol-gel method. *Appl. Phys. A Mater. Sci. Process.* **2020**, *126*, 552. [CrossRef]
40. Belka, R. Using the principal component analysis method in studies of the TiO_2 Raman spectra. In *Photonics Applications in Astronomy, Communications, Industry, and High Energy Physics Experiments*; Romaniuk, R.S., Linczuk, M., Eds.; SPIE: Bellingham, WA, USA, 2017; pp. 1415–1422.
41. Montenegro, D.N.; Hortelano, V.; Martínez, O.; Martínez-Tomas, M.C.; Sallet, V.; Muñoz-Sanjosé, V.; Jiménez, J. Non-radiative recombination centres in catalyst-free ZnO nanorods grown by atmospheric-metal organic chemical vapour deposition. *J. Phys. D. Appl. Phys.* **2013**, *46*, 235302. [CrossRef]
42. Yahia, S.B.; Znaidi, L.; Kanaev, A.; Petitet, J.P. Raman study of oriented ZnO thin films deposited by sol-gel method. *Spectrochim. Acta Part A Mol. Biomol. Spectrosc.* **2008**, *71*, 1234–1238. [CrossRef]
43. Muchuweni, E.; Sathiaraj, T.S.; Nyakotyo, H. Synthesis and characterization of zinc oxide thin films for optoelectronic applications. *Heliyon* **2017**, *3*, e00285. [CrossRef]
44. Tetteh, E.K.; Rathilal, S.; Naidoo, D.B. Photocatalytic degradation of oily waste and phenol from a local South Africa oil refinery wastewater using response methodology. *Sci. Rep.* **2020**, *10*, 8850. [CrossRef] [PubMed]
45. Lima, M.K.; Fernandes, D.M.; Silva, M.F.; Baesso, M.L.; Neto, A.M.; de Morais, G.R.; Nakamura, C.V.; de Oliveira Caleare, A.; Hechenleitner, A.A.W.; Pineda, E.A.G. Co-doped ZnO nanoparticles synthesized by an adapted sol–gel method: Effects on the structural, optical, photocatalytic and antibacterial properties. *J. Sol-Gel Sci. Technol.* **2014**, *72*, 301–309. [CrossRef]
46. Al-Ariki, S.; Yahya, N.A.A.; Al-A'nsi, S.A.; Jumali, M.H.H.; Jannah, A.N.; Abd-Shukor, R. Synthesis and comparative study on the structural and optical properties of ZnO doped with Ni and Ag nanopowders fabricated by sol gel technique. *Sci. Rep.* **2021**, *11*, 11948. [CrossRef] [PubMed]
47. Guo, X.; Zhang, Q.; Ding, X.; Shen, Q.; Wu, C.; Zhang, L.; Yang, H. Synthesis and application of several sol–gel-derived materials via sol–gel process combining with other technologies: A review. *J. Sol-Gel Sci. Technol.* **2016**, *79*, 328–358. [CrossRef]
48. Imbault, A.L.; Gong, J.; Farnood, R. Photocatalytic production of dihydroxyacetone from glycerol on TiO_2 in acetonitrile. *RSC Adv.* **2020**, *10*, 4956–4968. [CrossRef] [PubMed]
49. Vallejo, W.; Cantillo, A.; Salazar, B.; Diaz-Uribe, C.; Ramos, W.; Romero, E.; Hurtado, M. Comparative Study of ZnO Thin Films Doped with Transition Metals (Cu and Co) for Methylene Blue Photodegradation under Visible Irradiation. *Catalysts* **2020**, *10*, 528. [CrossRef]
50. Simmons, E.L. Relation of the Diffuse Reflectance Remission Function to the Fundamental Optical Parameters. *Opt. Acta Int. J. Opt.* **1972**, *19*, 845–851. [CrossRef]
51. Agarwal, S.; Jangir, L.K.; Rathore, K.S.; Kumar, M.; Awasthi, K. Morphology-dependent structural and optical properties of ZnO nanostructures. *Appl. Phys. A Mater. Sci. Process.* **2019**, *125*, 1–7. [CrossRef]
52. Sharma, D.K.; Shukla, S.; Sharma, K.K.; Kumar, V. A review on ZnO: Fundamental properties and applications. *Mater. Today Proc.* **2022**, *49*, 3028–3035. [CrossRef]
53. Mishra, V.; Warshi, M.K.; Sati, A.; Kumar, A.; Mishra, V.; Kumar, R.; Sagdeo, P.R. Investigation of temperature-dependent optical properties of TiO2 using diffuse reflectance spectroscopy. *SN Appl. Sci.* **2019**, *1*, 241. [CrossRef]
54. Staszak, M. A Linear Diffusion Model of Adsorption Kinetics at Fluid/Fluid Interfaces. *J. Surfactants Deterg.* **2016**, *19*, 297. [CrossRef]

55. McKay, G.; Parthasarathy, P.; Saleem, J.; Alherbawi, M.; Sajjad, S. Dye removal using biochars. In *Sustainable Biochar for Water and Wastewater Treatment*; Elsevier: Amsterdam, The Netherlands, 2022; pp. 429–471.
56. Gossard, A.; Frances, F.; Aloin, C. Rheological properties of TiO2 suspensions varied by shifting the electrostatic inter-particle interactions with an organic co-solvent. *Colloids Surf. A Physicochem. Eng. Asp.* **2017**, *522*, 425–432. [CrossRef]
57. Venu Rajendran, M.; Ganesan, S.; Sudhakaran Menon, V.; Raman, R.K.; Alagumalai, A.; Ashok Kumar, S.; Krishnamoorthy, A. Manganese Dopant-Induced Isoelectric Point Tuning of ZnO Electron Selective Layer Enable Improved Interface Stability in Cesium-Formamidinium-Based Planar Perovskite Solar Cells. *ACS Appl. Energy Mater.* **2022**, *5*, 6671–6686. [CrossRef]
58. Naseem, T.; Durrani, T. The role of some important metal oxide nanoparticles for wastewater and antibacterial applications: A review. *Environ. Chem. Ecotoxicol.* **2021**, *3*, 59–75. [CrossRef]
59. Di Mauro, A.; Landström, A.; Concina, I.; Impellizzeri, G.; Privitera, V.; Epifani, M. Surface modification by vanadium pentoxide turns oxide nanocrystals into powerful adsorbents of methylene blue. *J. Colloid Interface Sci.* **2019**, *533*, 369–374. [CrossRef]
60. Debnath, P.; Mondal, N.K. Effective removal of congo red dye from aqueous solution using biosynthesized zinc oxide nanoparticles. *Environ. Nanotechnol. Monit. Manag.* **2020**, *14*, 100320. [CrossRef]
61. Singh, K.K.; Senapati, K.K.; Sarma, K.C. Synthesis of superparamagnetic Fe3O4 nanoparticles coated with green tea polyphenols and their use for removal of dye pollutant from aqueous solution. *J. Environ. Chem. Eng.* **2017**, *5*, 2214–2221. [CrossRef]
62. Song, Z.; Chen, L.; Hu, J.; Richards, R. NiO(111) nanosheets as efficient and recyclable adsorbents for dye pollutant removal fromwastewater. *Nanotechnology* **2009**, *20*, 275707. [CrossRef] [PubMed]
63. Konicki, W.; Aleksandrzak, M.; Mijowska, E. Equilibrium, kinetic and thermodynamic studies on adsorption of cationic dyes from aqueous solutions using graphene oxide. *Chem. Eng. Res. Des.* **2017**, *123*, 35–49. [CrossRef]
64. Alalwan, H.A.; Mohammed, M.M.; Sultan, A.J.; Abbas, M.N.; Ibrahim, T.A.; Aljaafari, H.A.S.; Alminshid, A.A. Adsorption of methyl green stain from aqueous solutions using non-conventional adsorbent media: Isothermal kinetic and thermodynamic studies. *Bioresour. Technol. Rep.* **2021**, *14*, 100680. [CrossRef]
65. Bennabi, S.; Mahammed, N. Kinetic and Thermodynamic Study of Methyl Orange Dye Adsorption on Zinc Carbonyldiphthalate, an Organometallic-Based Material Prepared with a Montmorillonite Clay. *Iran. J. Chem. Eng.* **2023**, *42*, 1–123.
66. Darwish, A.A.A.; Rashad, M.; AL-Aoh, H.A. Methyl orange adsorption comparison on nanoparticles: Isotherm, kinetics, and thermodynamic studies. *Dye. Pigment.* **2019**, *160*, 563–571. [CrossRef]
67. Obulapuram, P.K.; Arfin, T.; Mohammad, F.; Khiste, S.K.; Chavali, M.; Albalawi, A.N.; Al-Lohedan, H.A. Adsorption, Equilibrium Isotherm, and Thermodynamic Studies towards the Removal of Reactive Orange 16 Dye Using Cu(I)-Polyaninile Composite. *Polymers* **2021**, *13*, 3490. [CrossRef]
68. Kinetics, N.; Badawi, A.K.; Emam, H.E.; Al-Harby, N.F.; Albahly, E.F.; Mohamed, N.A. Kinetics, Isotherm and Thermodynamic Studies for Efficient Adsorption of Congo Red Dye from Aqueous Solution onto Novel Cyanoguanidine-Modified Chitosan Adsorbent. *Polymers* **2021**, *13*, 4446.
69. Diaz-Uribe, C.; Walteros, L.; Duran, F.; Vallejo, W.; Romero Bohórquez, A.R. Prosopis juliflora Seed Waste as Biochar for the Removal of Blue Methylene: A Thermodynamic and Kinetic Study. *ACS Omega* **2022**, *7*, 42916–42925. [CrossRef] [PubMed]
70. Bedin, K.C.; Martins, A.C.; Cazetta, A.L.; Pezoti, O.; Almeida, V.C. KOH-activated carbon prepared from sucrose spherical carbon: Adsorption equilibrium, kinetic and thermodynamic studies for Methylene Blue removal. *Chem. Eng. J.* **2016**, *286*, 476–484. [CrossRef]
71. Al-Ghouti, M.A.; Al-Absi, R.S. Mechanistic understanding of the adsorption and thermodynamic aspects of cationic methylene blue dye onto cellulosic olive stones biomass from wastewater. *Sci. Rep.* **2020**, *10*, 15928. [CrossRef] [PubMed]